

## 3D Particle Tracking Velocimetry (PTV) Using High Speed Light Field Imaging

Abhishek Bajpayee<sup>1</sup> and Alexandra H. Techet<sup>2</sup>

Dept. of Mechanical Engineering, Massachusetts Institute of Technology, Cambridge, USA

<sup>1</sup> ab9@mit.edu

<sup>2</sup> ahtechet@mit.edu

### ABSTRACT

3D fluid flow visualization is of critical significance to a number of applications ranging from micro scale medical devices to design of ships and airplanes. Out of the various techniques currently used to visualize flow fields, particle image velocimetry (PIV) offers great advantages because it is negligibly intrusive and provides high resolution quantitative results. 2D and 3D PIV techniques are widely used in both research and industry and are of immense value, especially when high spatial and temporal resolutions can be achieved.

This paper extends Light Field (LF) imaging, the feasibility of using which for 3D PIV has been demonstrated by Belden et al [1], to 3D Particle Tracking Velocimetry (PTV), adding the ability to conduct Lagrangian studies on flow fields over time. For testing data, a rendering software was used to generate images that are nearly identical to actual images of a water tank seeded with PIV particles and illuminated by a volumetric laser. A thresholding and average intensity based particle search scheme is proposed to localize particles in the observation volume and then the relaxation tracking method is used to track the located particles in space across frames.

### 1. INTRODUCTION

The novel application of Light Field (LF) imaging to 3D Particle Imaging Velocimetry (PIV) and for bubble identification in Multi Phase flows was demonstrated by Belden et al in [1] and [2] respectively. They utilized the fact that LF imaging allows one to refocus at any arbitrary plane in the volume of interest to build accurate intensity volumes to be used for 3D cross correlation based PIV. This technique and has several advantages as a fluid flow imaging technique. It allows an out of plane resolvable (Z) dimension of the same order as the in plane (X-Y) dimension and facilitates seeing through some occlusions in the scene thus increasing spatial resolvability of particles/features. It also performs better than most other technologies with densely seeded flows. Authors of [1] used an array of up to 10 cameras that provided a maximum of 30 frames per second and were able to demonstrate the ability to spatially resolve densely seeded velocity fields with great accuracy.

PIV however, even when performed over time, only provides Eulerian information about the flow and thus restricts one from performing studies, such as analysis of fluid mixing, which require Lagrangian information about the flow field which cannot be extracted directly from PIV data. This is because PIV techniques, mostly cross correlation based, require only gray-level images (for 2D) or intensity fields (for 3D) and do not require determination of individual particle locations which is a prerequisite to track particles, be it in a plane or in a volume.

In the past decade, PTV in 3D has been demonstrated by Pereira et al [3] for use with the defocusing digital particle image velocimetry (DDPIV) technique, by Hoyer et al [5] using 3D scanning particle tracking velocimetry (SPTV), by Satake et al [6] and Kim et al [7] using micro digital holographic particle tracking velocimetry (micro-DHPTV). Authors of [3] were able to accurately track 5000 synthetically generated particles for a simple Burgers' vortex flow and for a more complex multi-scale vortical flow. Authors of [5] were able to track 3500 particles in a turbulent flow field using a single high speed camera. Authors of [6] were able to track 140 particles per frame in a micro tube. DDPIV and SPTV are able to achieve a very high spatial resolution. SPTV however is restricted to lower speed flows.

In this paper, the authors demonstrate the applicability of LF imaging to 3D PTV. A new thresholding and average intensity based particle search scheme is proposed, which on a 2D level is based on a particle detection technique, similar to dynamic threshold binarization proposed by Ohmi et al [4], but is extended and further developed to facilitate accurate 3D localization of particles in the observation volume. The particles once located in space can then be tracked using several methods such as nearest neighbor, neural networks, the relaxation method, variational method etc. depending on seeding density and average velocity in the tracking region. For the purpose of this study however, only the relaxation method was used.

### 2. REFOCUSING

Using LF imaging principles, one can calculate an image by combining images from all cameras being used in the setup (Fig. 2) such that the resulting image is sharply focused at an arbitrary depth in the scene. In this study, the focus is changed such that the focal plane is always perpendicular to the z axis. Since this focusing is achieved by combining images from discrete cameras and not from a real large aperture lens, objects in the refocused image that do not lie on the focal plane have a discrete blur (as shown in Fig. 1). Once the images from each camera have been transformed and shifted to correct for difference in point of view of each camera they can be

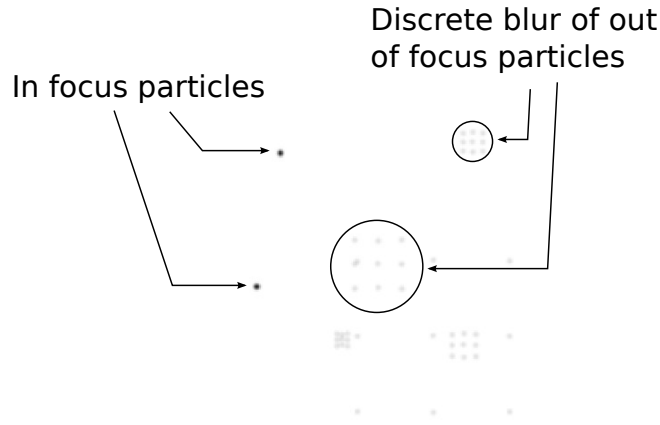


**Figure 1:** An example of what the discrete blur of out of focus particles looks like. The picture has been inverted to increase visibility.

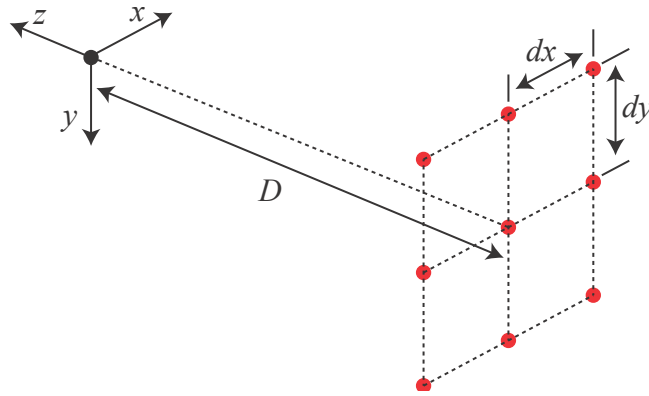


**Figure 2:** Schematic of camera array and scene setup. Red dots indicate camera locations. All cameras are pointed at the origin.

combined using either an additive method (Eqn. 1) or using a multiplicative method (Eqn. 2).

$$I_{refocused} = \sum_{i=1}^N \frac{1}{N} I_i \quad (1)$$

$$I_{refocused} = \prod_{i=1}^N I_i^\alpha \quad (2)$$

where  $I_i$  is the image from camera  $i$  (after being transformed and shifted),  $N$  is the number of cameras being using and  $\alpha$  (in Eqn. 2 is a factor that each image  $I_i$  is raised to. An  $\alpha$  of  $1/N$  ( $N=9$ ) was used in this study.

Since each image is either divided by  $N$  or raised to the power  $1/N$ , the discrete blur of every out of focus image has an intensity much lower than the intensity the particle has in the original image. These particles can easily be removed by thresholding an image to an appropriate extent such that the intensity of every pixel below a certain intensity level is set to zero. When a multiplicative method is used to refocus however, the blur is automatically removed because the pixels representing the blur of an out of focus particle are multiplied by the pixels in another image that are black. This thresholded image then only has particles visible that are in or almost in focus at the given  $z$  depth and thus can then be used to search for particles using algorithms used for 2D PIV data.

### 3. PARTICLE LOCALIZATION

#### 3.1 2D Particle Detection

Several particle detection techniques have been developed for use in 2D PTV which look for particles in images based on the fact that particles in grayscale PIV data look like a group of gray or white pixels. The dynamic threshold binarization technique [4] proposed by Ohmi et al has been shown to be very effective in searching even for particles that have different intensity levels. A similar technique is used to detect particles in the images but without using any thresholding. This is because the images in which particles are being detected have already been thresholded to get rid of blurred particles and this also gets rid of background noise and essentially renders the background black.

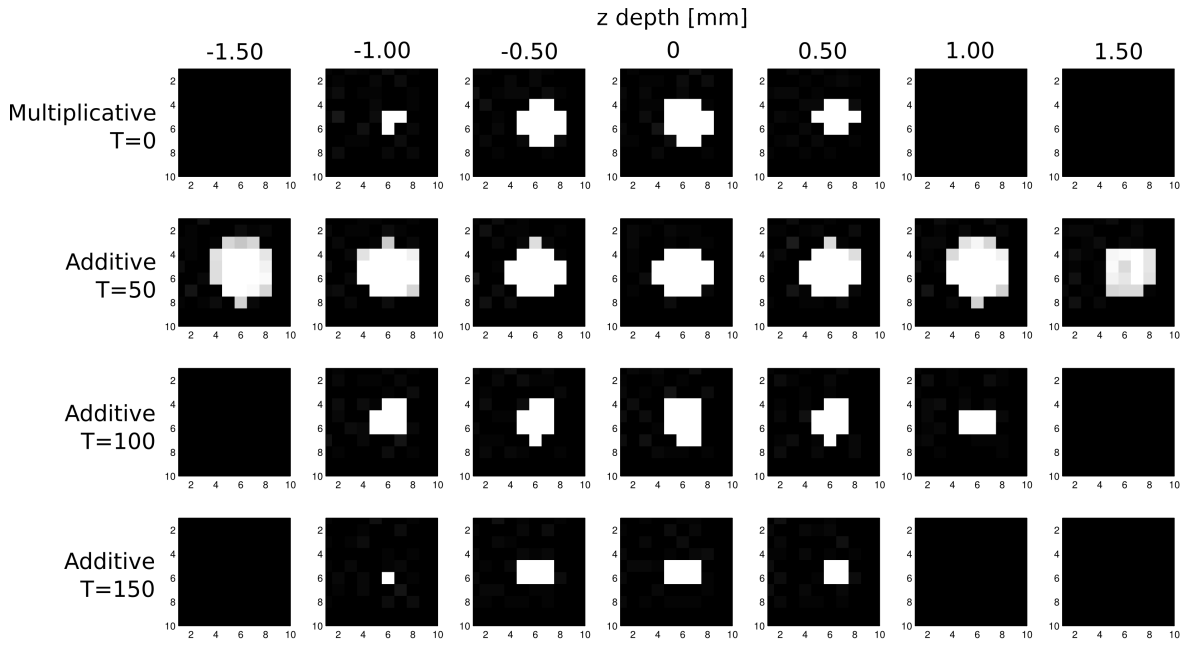
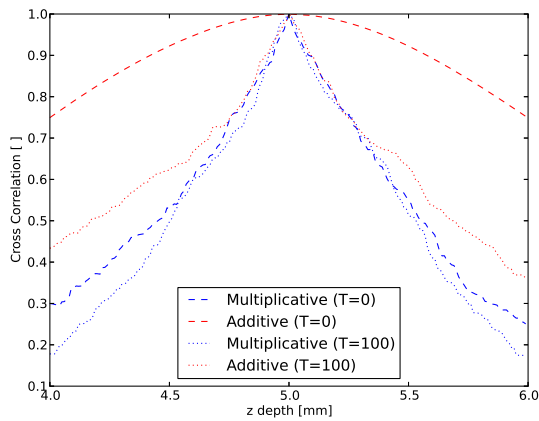


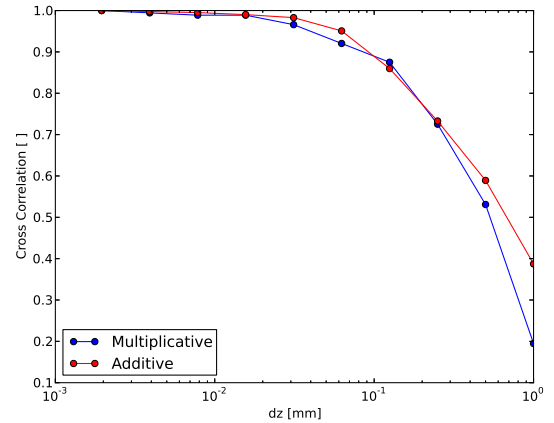
**Figure 3:** A particle located at  $z=0$  as it goes in and out of focus using different refocusing methods.  $T$  is the threshold level.

The algorithm implemented only looks for intensity peaks in the image and then converges to the local maximum of each such peak to find the particle centroid. An assumption about the minimum size of each particle is made to further get rid of apparent particles that might be noise or ghosts.

### 3.2 3D Location Inference



(a) Given image refocused at  $z$ .  $T$  is the threshold level used.



(b) Given image refocused at  $dz$  away from  $z_{ref}$ . Threshold level of 90 was used for additive method.

**Figure 4:** Cross correlation between given image and an image refocused at a reference depth  $z_{ref}$  of 5 mm.

As one changes the focus through the investigation volume using synthetic refocusing, each particle goes in and out of focus as shown in Fig. 3. 2D particle detection, as outlined in the previous subsection, is performed on the refocused images for the entire volume using a small  $dz$  between each focal plane. The  $dz$  that can be used has a lower bound that depends on the baseline spacing ( $dx$  and  $dy$  as shown in Fig. 2) between the cameras and the distance of the camera array from the investigation volume ( $D$  in Fig. 2). Fig 4(a) shows a plot of cross correlation between an image refocused at a given  $z$  depth with an image refocused at a reference depth  $z_{ref}$  of 5 mm. Fig 4(b) shows a plot of cross correlation between an image refocused  $dz$  away from  $z_{ref}$  with an image refocused at  $z_{ref}$ . Results using both additive and multiplicative refocusing methods are shown. Fig. 4(b) shows that the images can be refocused a very small  $dz$  (as low as 0.01 mm) apart and still have a detectable difference between them showing that the technique provides a very high resolution in the  $z$  direction. Fig. 4(a) shows that thresholding does not affect the resolvability for multiplicative refocusing and that multiplicative refocusing is very similar to additive refocusing followed by thresholding.

After identifying particles in each refocused image, one can obtain the x, y and z coordinates of particles where the x and y coordinates are derived from the 2D location of the particle in an image and the z coordinate is the depth at which the focus of the image lies in which particles are being detected. As a result, one can obtain a cloud of points where tight point clusters represent actual particles in space. Points in these clusters can be grouped together and then used to calculate the locations of particles in space. In each such cluster, points differ slightly in x and y coordinates and in average intensity over z. To calculate the x and y coordinates for the particle, the x and y coordinates at each z depth are simply averaged. Each particle is generally in focus over a range in the z direction which is considerably larger than its actual extent in space. The z coordinate can thus be obtained either by calculating the mean of the minimum and maximum z depths at which the particle becomes visible and ceases to be visible respectively or by fitting a gaussian function to the intensity distribution over z and finding its peak location. Fig. 6 shows the normalized intensity variation of a particle vs. its depth in volume and shows that the average intensity of a particle follows a roughly gaussian trend with change in z depth. Since any particle is visible over about 3 mm of change in z depth, multiple particles having nearly identical x and y coordinates lying 1.5 mm or less apart in z depth are interpreted as one particle. This situation however, is unlikely to occur in a seeded tank that is well mixed.

To test the accuracy of particle localization in space, a case was rendered with 125 points in a 5 x 5 x 5 grid centered at the origin. All 125 points were detected using both additive (threshold of 90) and multiplicative refocusing methods. The average localization error defined as:

$$\epsilon_{localization} = \frac{1}{n} \sum_i^n |x_i^{(detected)} - x_i^{(actual)}| \quad (3)$$

where n is the number of particles being compared was found to be 0.2177 mm for additive refocusing and 0.2231 mm for multiplicative refocusing. Fig 5 shows a comparison of how well the particle detection and localization scheme performs by comparing number of detected particles with the actual number of seeded particles. It can be seen that a threshold of 50 is too low when additive refocusing is used as it leads to detection of ghosts as particles. Also a threshold of 150 is too high as it ends up removing some actual particles from the images. Additive refocusing however performs well using a threshold of 90. Multiplicative refocusing seems to perform well but for only some cases. The reason why this happens is under investigation.

The refocusing and particle detection code has been developed to utilize a CUDA capable GPU for most computations that can be parallelized to help greatly increase the computation speed in order to facilitate processing of high speed data (recorded at up to 3200 Hz) in a relatively short amount of time.

#### 4. PARTICLE TRACKING

Once 3D particle locations are obtained for a sequence of images over time, their movement can be tracked. The key parameters that affect the performance of a particular tracking method are the seeding density and the distance moved by the particles between each successive frame. In this study, the relaxation method was used to track the particles. The relaxation method was first proposed by Barnard and Thompson [9] and was first implemented for 2D particle tracking in fluid mechanics by Baek and Lee [10]. Pereira and Jia ([3], [8]) discuss this technique in extensive detail.

The relaxation method is an iterative method which uses constraints derived from known aspects about the flow such as flow similarity, velocity, etc. The first step in implementing this method is to build reference and candidate sets  $S_r$  and  $S_c$  respectively such that:

$$S_r = \{x_k : |x_i - x_k| < R_n\} \quad (4)$$

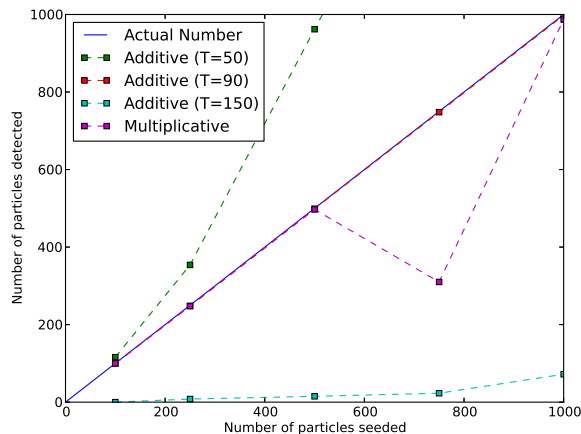
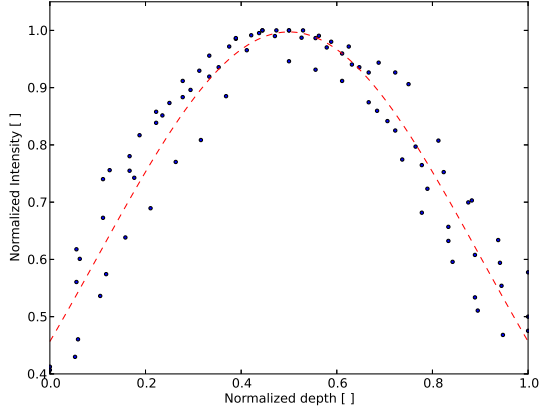
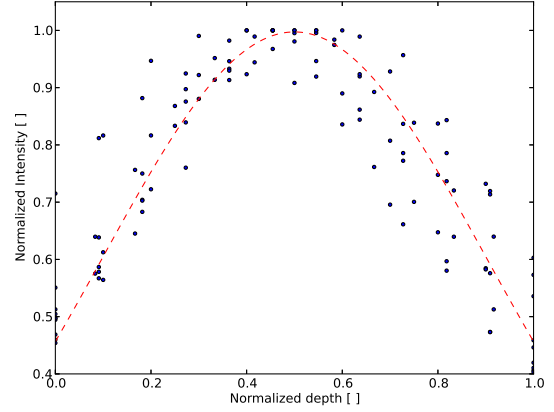


Figure 5: Number of particles detected using different schemes vs. the actual number of particles seeded in the volume.



(a) Using additive refocusing



(b) Using multiplicative refocusing

**Figure 6:** Normalized intensity of particle vs. normalized z depth in volume. The dashed red line is an approximate fit normal distribution curve with  $\mu$  of 0.5 mm and  $\sigma$  of 0.4mm.

$$S_c = \{y_j : |x_i - y_j| < R_s\} \quad (5)$$

where  $x_i$  is the location of a particle in the first frame and  $y_j$  is the location of a particle in the second frame,  $R_n$  is the neighborhood threshold and  $R_s$  is the maximum movement threshold. Once these sets have been established for each particle  $x_i$ , the next step is to find the most probable matching particle in  $S_r$  for each particle in  $S_c$ . This is achieved by defining a matching probability  $P_{ij}$  between each particle  $i$  in  $S_r$  and particle  $j$  in  $S_c$ . In addition for particle  $i$  in  $S_r$  is defined a probability  $P_i$  that particle  $i$  has no match in  $S_c$ . These probabilities must satisfy the following condition:

$$\sum_{i \in S_r, j \in S_c} P_{ij} + P_i = 1 \quad (6)$$

and are initialized as:

$$P_{ij}^{(0)} = P_i^{(0)} = 1/(M_i + 1) \quad (7)$$

where  $M_i$  is the number of particles in  $S_c$  and the superscript indicates the iteration number. After this initialization the probabilities are iteratively updated as:

$$P_{ij}^{(n)} = P_{ij}^{(n-1)} \left( A + B \sum_{k,l \in \Theta} P_{kl}^{(n-1)} \right) \quad (8)$$

$$\Theta = \{(k,l) : |d_{ij} - d_{kl}| < E + F|d_{ij}|\} \quad (9)$$

where A and B are weighting constants (A=0.3 and B=3.0 [9], [4]), and  $d_{ij} = x_i - y_j$  and  $d_{kl} = x_k - y_l$ . E and F are constants that determine the relaxation area that enforces a non rigid directional flow similarity constraint (E=1.0 and F=0.05 [4]). The last step of each loop is to normalize all probabilities such that they satisfy Eqn. 6:

$$P_{ij}^{(n)} = \frac{P_{ij}^{(n)}}{\sum_j P_{ij}^{(n)} + P_i^{(n)}} \quad (10)$$

$$P_i^{(n)} = \frac{P_i^{(n)}}{\sum_j P_{ij}^{(n)} + P_i^{(n)}} \quad (11)$$

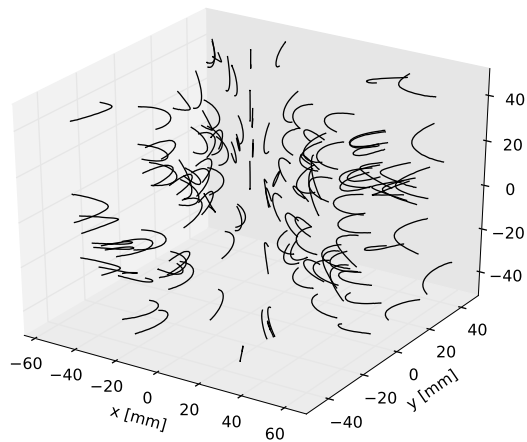


**Figure 7:** Particle trajectories found after tracking. Only particles that were visible over the entire 1 second duration are shown and only a third of the total number of particles trajectories are shown to improve visibility.

The match probabilities generally converge in about 10 to 20 iterations. Note that since this tracking method works on only two consecutive frames at a time, particles coming into the volume and leaving the volume can be tracked for only the part of the duration over which they are in the investigation volume.

To test the tracking algorithm, a case was generated with 1500 particles randomly seeded between -75 mm and 75 mm in all three directions around the origin. These particles were propagated over 1 second at 30 Hz in the volume according to a flow field determined by a vortex ring of radius 37.5 mm lying in the xy plane and moving in the z direction such that it moves across the investigation volume in 1 second. The number of particles detected in each frame ranged between 420 and 480. This is because a lot of particles initially seeded were outside the field of view of the cameras. Out of all the particles tracked, 366 were visible over the entire 1 second duration. Fig. 7 shows the trajectories of these particles. It is visually evident that the tracking algorithm was able to find the correct matches across all frames.

The complexity of solving the tracking problem increases with increase in seeding density and the average distance moved by particles between recorded frames. The limits of the algorithm however are still under investigation.

## 5. CONCLUSION

It is shown that LF imaging can be used to resolve the 3D location of particles to a high accuracy that can then be tracked in space over time. This provides high resolution Lagrangian information about the flow and can be used to study aspects that cannot be studied using PIV.

Not only is LF imaging based PTV accurate, it is also much faster than existing methods of PIV and PTV using the code developed by the authors. Experimental benchmarking of the code is yet to be conducted. In addition, an LF PTV setup is minimally intrusive to the experimental location since it looks at the investigation volume from only one direction as compared to some other technologies. It can thus be concluded that LF PTV is a technology that has great promise as a 3D flow study tool and can help both industry and research.

## 6. ACKNOWLEDGEMENTS

The authors are grateful for the generous funding from ONR (Grant #N00014-12-1-0787, Dr Steven Russell) and the Naval Engineering Education Center. The authors are also grateful to other members of the Experimental Hydrodynamics Lab at MIT, Leah Mendelson and Barry Scharfman, for helpful discussions and insights. Lastly, the authors are grateful to the developers of open source tools such as Blender [11] (a free 3D rendering application), OpenCV [12] (a computer vision library), and Ceres Solver [13] (a nonlinear least squares solver) which were critical to the development of the method presented in this paper.

## REFERENCES

- [1] Belden J., Truscott T.T., Axiak M.C., and Techet A.H., Three-dimensional synthetic aperture particle image velocimetry, *Measurement Science and Technology* 21 (2010) 125403 pp. 21
- [2] Belden J., Ravela S., Truscott T.T., and Techet A.H., Three-dimensional bubble field resolution using synthetic aperture imaging: application to a plunging jet, *Experiments in Fluids* (2012) 53: 839-869

- [3] Pereira F., Ster H., Graff E.C., and Gharib M., Two-frame 3D particle tracking, *Measurement Science and Technology* 17 (2006) 1680-1692
- [4] Ohmi K., and Li H., "Particle-tracking velocimetry with new algorithms", *Measurement Science and Technology* 11 (2000) 603-616
- [5] Hoyer K., Holzner M., Lthi B., Guala M., Liberzon A., and Kinzelbach W., "3D scanning particle tracking velocimetry", *Experiments in Fluids* (2005) 39: 923-934
- [6] Satake S., Kunugi T., Sato K., Ito T., Kanamori H., Taniguchi J., "Measurement of 3D flow in a micro-pipe via micro digital holographic particle tracking velocimetry", *Measurement Science and Technology*, 17 (2006) 1647-1651
- [7] Kim S., and Lee S.J., "Measurement of 3D laminar flow inside a micro tube using micro digital holographic particle tracking velocimetry", *Journal of Micromechanics and Microengineering*, 17 (2007) 2157-2162
- [8] Jia P., Wang Y., Zhang Y., "Improvement in the independence of relaxation method-based particle tracking velocimetry", *Measurement Science and Technology*, 24 (2013) 055301 (13pp)
- [9] Barnard S.T. and Thompson W.B., "Disparity Analysis of Images", *IEEE Transactions on Pattern Analysis and Machine Intelligence*, 2 (1980) 333-340
- [10] Baek S.J. and Lee S.J., "A new two-frame particle tracking algorithm using match probability", *Experiments in Fluids*, 22 (1996) 23-32
- [11] Blender 3D Creation Software, <http://www.blender.org/>
- [12] Open Source Computer Vision, <http://opencv.org/>
- [13] Agarwal S. and Mierle K., "Ceres Solver: Tutorial & Reference", Google Inc.